International Journal of Nanomedicine

Dovepress
Taylor & Francis Group

Open Access Full Text Article

ORIGINAL RESEARCH

Bioactive Platinum Nanozymes Accelerate Diabetic Wound Healing via Anti-Inflammation and Macrophage Polarization Modulation

Liyong Shi[1,*], Jing Cheng[2,*], Lianshun Lin[1,*], Tanwei Liu[1], Linlin Chen[2], Xiali Wang[2], Suqin Cai[3], Liliang Qiu[1], Miaoxiang Chen[1], Qidong Chen[1], Fanbin Zhong[1], Furong Yan[4], Xiaoyang Chen[1], Yiming Zeng[1]

[1]Department of Pulmonary and Critical Care Medicine, the Second Affiliated Hospital of Fujian Medical University, Quanzhou, 362000, People's Republic of China; [2]Department of Clinical Medicine, Quanzhou Medical College, Quanzhou, 362000, People's Republic of China; [3]Department of Pathology, the Second Affiliated Hospital of Fujian Medical University, Quanzhou, 362000, People's Republic of China; [4]Center of Molecular Diagnosis and Therapy, the Second Affiliated Hospital of Fujian Medical University, Quanzhou, 362000, People's Republic of China

*These authors contributed equally to this work

Correspondence: Xiaoyang Chen; Yiming Zeng, Department of Pulmonary and Critical Care Medicine, the Second Affiliated Hospital of Fujian Medical University, Quanzhou, 362000, People's Republic of China, Email ccxxyy008@fjmu.edu.cn; zeng_yi_ming@126.com

Purpose: This study aims to develop a therapeutic agent that accelerates the healing of chronic diabetic wounds by harnessing the highly efficient enzyme-mimicking activity of platinum nanozymes, and to elucidate its underlying mechanisms, thereby offering new insights for the treatment of diabetic wounds.

Methods: SHA-PtNPs were synthesized using sodium hyaluronate (SHA) as the carrier, and their structural features were characterized by XRD, TEM, XPS and FTIR. The composite was then applied to evaluate wound-healing efficacy in diabetic mice. Furthermore, H&E staining, immunofluorescence staining, and other analyses were employed to investigate its underlying mechanisms in promoting wound repair.

Results: The results revealed that SHA-PtNPs significantly accelerated wound closure through multiple mechanisms: (1) effective suppression of inflammatory responses and related cytokine production; (2) promotion of TGF-β1 secretion and upregulation of CD31 and α-SMA expression, thereby enhancing angiogenesis and tissue contraction; and (3) induction of macrophage polarization from the pro-inflammatory M1 phenotype to the pro-healing M2 phenotype.

Conclusion: These findings suggest that SHA-PtNPs, as a nanozyme-based material, hold great potential as an efficient therapeutic agent for diabetic wound healing, demonstrating a synergistic mechanism that integrates ROS regulation with immune microenvironment modulation.

Keywords: platinum, nanozyme, anti-inflammation, skin wound, macrophage polarization

Introduction

Diabetes mellitus is a common endocrine disorder characterized by chronic hyperglycemia.[1] Prolonged high blood glucose levels can cause vascular endothelial damage, leading to both microvascular and macrovascular complications, thereby reducing blood supply to wound sites and impairing the delivery of oxygen, nutrients, and immune cells. In addition, hyperglycemia often induces peripheral neuropathy, resulting in sensory impairment that may cause patients to neglect wounds and increase the risk of infection.[2,3] Glucose also serves as a favorable nutrient source for microorganisms, and the hyperglycemic environment facilitates the proliferation of bacteria (such as *Staphylococcus aureus* and *Pseudomonas aeruginosa*) and fungi. These pathogens can easily form biofilms on wound surfaces, resisting antibiotics and immune clearance.[4–6] Consequently, diabetic complications are among the major causes of mortality in diabetic patients. Among these complications, chronic diabetic wounds are characterized by persistent inflammation, nutritional

https://doi.org/10.2147/IJN.S586975
Received: 21 December 2025
Accepted: 5 March 2026
Published: 10 March 2026

Graphical Abstract

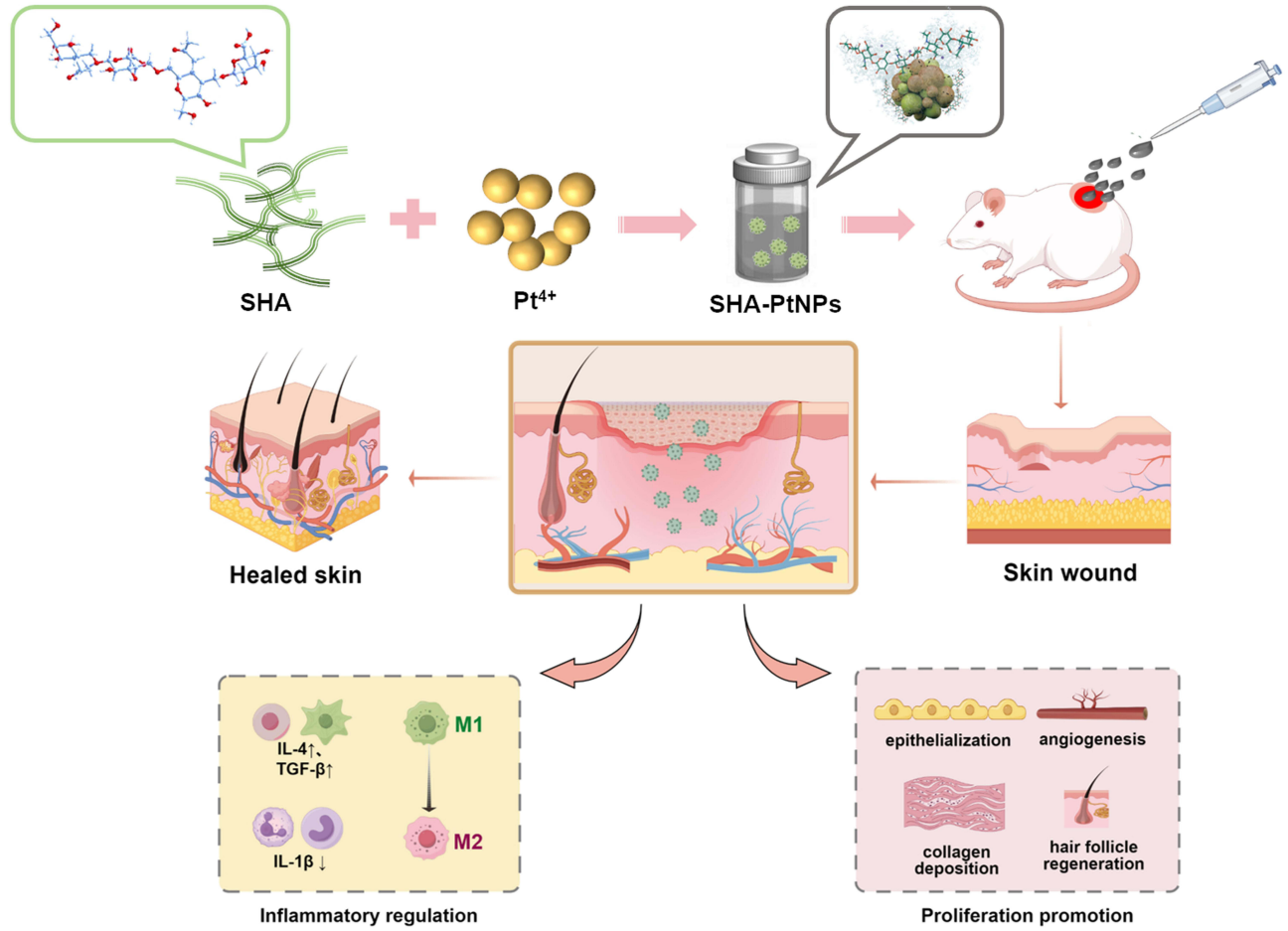

deficiency, and hypoxia. Sustained inflammation can trigger excessive oxidative stress, during which overproduction of reactive oxygen species (ROS), particularly superoxide anions and hydrogen peroxide-leads to lipid peroxidation, DNA oxidation, and protein damage. These processes severely inhibit cell proliferation and migration, ultimately delaying wound healing. Therefore, the development of effective therapies for non-healing diabetic wounds is of great importance. Antioxidant therapy represents a promising strategy, as introducing antioxidant materials to eliminate excess ROS can alleviate inflammation and accelerate wound repair.[7–10] For example, Zhang et al reported an SSD-PG-PVA/KGM fibrous membrane that effectively scavenged ROS through the intrinsic antioxidant properties of PG, promoting diabetic wound healing.[11] Although various wound-healing materials, such as functional dressings based on natural antioxidants (eg, polyphenols and vitamins) and drug-loaded hydrogels, have been developed for diabetic wound treatment, they still exhibit certain limitations.[12,13] Natural antioxidants are prone to degradation and inactivation under pathological conditions, and their release rates often fail to maintain effective concentrations over time.[14,15] Some metal ions or metal oxides possess antibacterial properties but may simultaneously induce excessive ROS generation, aggravating oxidative stress.[16–18] Conventional polymer hydrogels or fibrous membranes can maintain a moist wound environment but lack the capability to specifically regulate the redox balance.[19–22] Therefore, it is urgently necessary to develop functional materials that can maintain stable activity in complex wound environments and coordinate the regulation of inflammation and oxidative stress through multiple mechanisms.[23,24]

Nanozymes are a class of nanomaterials that possess enzyme-mimicking catalytic activities and can catalyze specific substrate reactions under appropriate conditions.[25] They can simulate the functions of various natural enzymes, such as superoxide dismutase (SOD), catalase (CAT), and glutathione peroxidase (GPx). Compared with natural enzymes, nanozymes exhibit several advantages, including multi-enzyme activities, tunable regulation of ROS, high surface area, structural design flexibility, and excellent stability. These properties have enabled their extensive applications in catalysis, biosensing, and bioimaging.[26–31] In the context of wound healing, nanozymes can maintain stable catalytic performance in complex wound environments, effectively scavenge excessive ROS, and exhibit multifunctional effects such as antioxidant, anti-inflammatory, and antibacterial activities through rational structural and surface design. Owing to their potent ROS scavenging capability, nanozymes have been reported to alleviate oxidative stress, suppress inflammation, and treat ROS-related diseases, highlighting their great potential in promoting chronic wound repair.[32–35]

Our previous studies revealed that the designed and synthesized SHA-PtNPs possesses both bioactivity and enzyme-like catalytic properties, exhibiting remarkable CAT and SOD activities capable of efficiently scavenging ROS.[25] Based on these findings, we employed SHA-PtNPs as a material for the treatment of diabetic wounds in therapeutic applications. The results indicated that this material effectively eliminates excessive ROS within the wound microenvironment, alleviating inflammation, promoting angiogenesis and cell migration, and ultimately accelerating the healing of diabetic wounds. Compared with therapeutic strategies relying on a single mode of action, the SHA-PtNPs system enables multidimensional and synergistic regulation of oxidative stress, the immune microenvironment, macrophage phenotype transition, and angiogenesis, thereby establishing a more integrated, systematic, and efficient therapeutic mechanism.[36–38] This study provides a valuable strategy and experimental foundation for the development of nanozyme-based biomaterials for chronic wound therapy.

Materials and Methods

Materials and Reagents

Main materials including sodium hyaluronate (SHA) (from Streptococcus Equi, 95% purity, the molecular weight of 1,350,000–1,650,000 Da; Macklin Biochemical Tech), sodium borohydride ($NaBH_4$; Sinopharm Chemical Reagent), chloroplatinic acid (H_2PtCl_6; Aladdin Chemistry), anti-IL-4, anti-IL-1β, anti-CD31, anti-α-SMA and anti-TGF-β1 (Thermo Fisher Scientific), Hematoxylin and Eosin (H&E) staining kit, Masson staining kit and DPAI (Beyotime), anti-CD68, anti-CD206 and anti-CD86 (Proteintech) were used. All solutions were prepared using deionized water.

Preparation of SHA-PtNPs

The preparation of SHA-PtNPs was carried out according to our previous work.[25] Briefly, 0.2 g of sodium hyaluronate (SHA) was dissolved in 50 mL of deionized water under stirring until completely dissolved (approximately 15 min). Then, 47 mL of the SHA solution was transferred and mixed with 2 mL of H_2PtCl_6 solution (10 mmol/L) under light-protected stirring at room temperature for 30 min. Subsequently, 1 mL of freshly prepared $NaBH_4$ solution (60 mmol/L) was added dropwise within 5 min under vigorous stirring. The reaction was continued for 90 min under dark conditions. The obtained SHA-PtNPs were stored at 4 °C in the dark until further use. The final SHA-PtNPs dispersion had a total concentration of 3.8 mg/mL, with platinum and SHA contents of 0.078 mg/mL and approximately 3.8 mg/mL, respectively.

Establishment of a Rat Model of Chronic Wounds

Male Sprague-Dawley (SD) rats (8 weeks old, n = 24) were used in this study. After one week of acclimatization, the animals were randomly divided into three groups: control (CON), SHA, and SHA-PtNPs groups. All animals' protocols were approved by the Research Ethics Committee of the second Affiliated Hospital of Fujian Medical University (Approval ID: 2022–544) and complied with the National Institutes of Health Guidelines for the Care and Use of Laboratory Animals. Diabetes was induced by intraperitoneal injection of streptozotocin (STZ, 45 mg/kg). Blood glucose levels were measured from the tail vein at 24 hours and 72 hours post-injection, and rats with blood glucose levels exceeding 16.7 mmol/L were considered successfully diabetic.

After successful model establishment, SD rats were anesthetized by intraperitoneal injection of 2% sodium pentobarbital (40 mg/kg). The dorsal hair was shaved, and a full-thickness circular skin wound (15 mm in diameter) was created on the dorsal area, extending down to the fascia. According to the grouping, 150 μL of normal saline (NS) (0.9%), SHA solution, or SHA-PtNPs suspension was applied topically to the wound. The treatment was administered once daily for the first three days and then every other day thereafter. Rats were housed individually after surgery and the wounds were photographed at predetermined time points. The percentage of wound closure was calculated as follows: Wound closure rate$(\%) = \frac{A0-At}{A0} \times 100\%$, where A_0 represents the initial wound area and A_t represents the unhealed wound area at each time point. Skin tissue samples were collected on days 3, 9, 12, 15, and 28. Portions of each sample were stored at −80 °C for biochemical analysis, and the remaining tissues were fixed in formalin for histological examination. After all of the experiment, SD rats were euthanized by intraperitoneal injection of 2% sodium pentobarbital (120 mg/kg), and death was confirmed by multiple criteria, including cessation of heartbeat, respiration, and reflexes.

Inflammation Scoring

We have conducted a semi-quantitative histopathological scoring for the degree of inflammatory cell infiltration in H&E stained sections, based on established criteria.[39] An established semi-quantitative scoring system based on the density of inflammatory cells was employed: Score 0: No or minimal inflammatory cell infiltration; Score 1 (Mild), Scattered or focal presence of a small number of inflammatory cells; Score 2 (Moderate), Moderate inflammatory cell infiltration, forming distinct inflammatory foci; Score 3 (Severe), Extensive, diffuse inflammatory cell infiltration, possibly accompanied by abscess formation. Two pathologists who were blinded to the experimental groups, performed the scoring independently. Each tissue section was observed and scored in at least five different non-overlapping high-power fields (20× magnification). The average score from all fields was calculated as the final score for that section.

Histological Analysis

For immunohistochemical (IHC) analysis, the rat wound tissues were collected from each group on day 3, 9, 15 and 28 post-treatments, which were fixed, paraffin-embedded and cut into 5-μm slices. Embedded tissue sections were stained with H&E staining and Masson's trichrome (MT) staining. Additionally, the expressions of healed wound tissue sections were also stained with IL-4, IL-1β, TGF-β1, CD 31 and α-SMA IHC staining on day 3 and day 9.

Immunofluorescence Staining

To visualize the regulation of macrophage polarization by SHA-PtNPs in wound healing, skin tissue sections were rinsed with NS and blocked with goat serum at room temperature on day 3 and day 15 post-treatment. The phenotypic analysis of macrophages was performed using TSA-based double immunofluorescence staining. CD68 was employed as a pan-macrophage marker to identify the macrophage population. CD86 and CD206 served as specific markers for M1 and M2 macrophages, respectively. Accordingly, we performed dual staining for M1 Macrophages: CD68 and CD86; M2 Macrophages: CD68 and CD206. Following image acquisition, the quantification was performed using Image J software. The fluorescence intensity of CD86 and CD206 was measured in regions of interest corresponding to CD68-positive cells. The CD206/CD86 ratio was then calculated from these intensity values. This ratio was used as an indicator to assess the relative balance or shift between M1 and M2 macrophage phenotypes.

Statistical Analysis

Data analysis was conducted using GraphPad Prism 8.0 and SPSS 26.0. The collected data were presented as mean ± standard deviation (SD). For statistical significance of differences between two groups, a Student's *t*-test was used, while one-way analysis of variance (ANOVA) followed by Tukey's post hoc test was applied for multiple group comparisons. Statistical significance was set at $P < 0.05$.

Results and Discussion

Characterization of SHA-PtNPs

The synthesis of SHA-PtNPs was carried out following our previous protocol. The obtained SHA-PtNPs were subsequently characterized to confirm their structural and physicochemical properties. Transmission electron microscopy (TEM) images revealed that the PtNPs were uniformly dispersed within the SHA matrix, exhibiting a well-defined spherical morphology (Figure 1A), consistent with our earlier findings. X-ray photoelectron spectroscopy (XPS) analysis showed the characteristic binding energy peaks of the main elements (C, N, O, and Pt) in the SHA-PtNPs powder (Figure 1B). In the Pt spectrum, two distinct peaks corresponding to Pt $4f_7/_2$ and Pt $4f_5/_2$ were observed, indicating the coexistence of Pt^0 and Pt^{4+} species (Figure S1). The X-ray diffraction (XRD) pattern (Figure 1C) further confirmed the crystalline structure of Pt, with diffraction peaks matching those of standard Pt according to JCPDS card No. 87–0640. Furthermore, Fourier-transform infrared spectroscopy (FTIR) analysis demonstrated characteristic shifts after coordination with SHA. The stretching vibration peaks of -COO- originally observed at 1616 cm^{-1} and 1410 cm^{-1} shifted to 1618 cm^{-1} and 1412 cm^{-1}, respectively, while the -C-OH stretching vibration at 1042 cm^{-1} also exhibited a slight shift (Figure 1D). These results confirm the successful synthesis of SHA-PtNPs.

Wound-Healing Performance of SHA-PtNPs

Our previous studies demonstrated that SHA-PtNPs exhibit multiple enzyme-mimicking activities. Specifically, SHA-PtNPs showed CAT-like activity, catalyzing the decomposition of H_2O_2 into harmless oxygen and water with an activity of 3320 U/g. In addition, SHA-PtNPs exhibited remarkable SOD-like activity, converting superoxide anions into H_2O_2 and oxygen, followed by further decomposition of the generated H_2O_2 via their CAT-like activity, with an overall activity of 129,000 U/g. Moreover, SHA-PtNPs were also capable of scavenging hydroxyl radicals to a certain extent.[25] Based on these promising findings, we hypothesized that SHA-PtNPs possess strong antioxidant properties that could contribute to

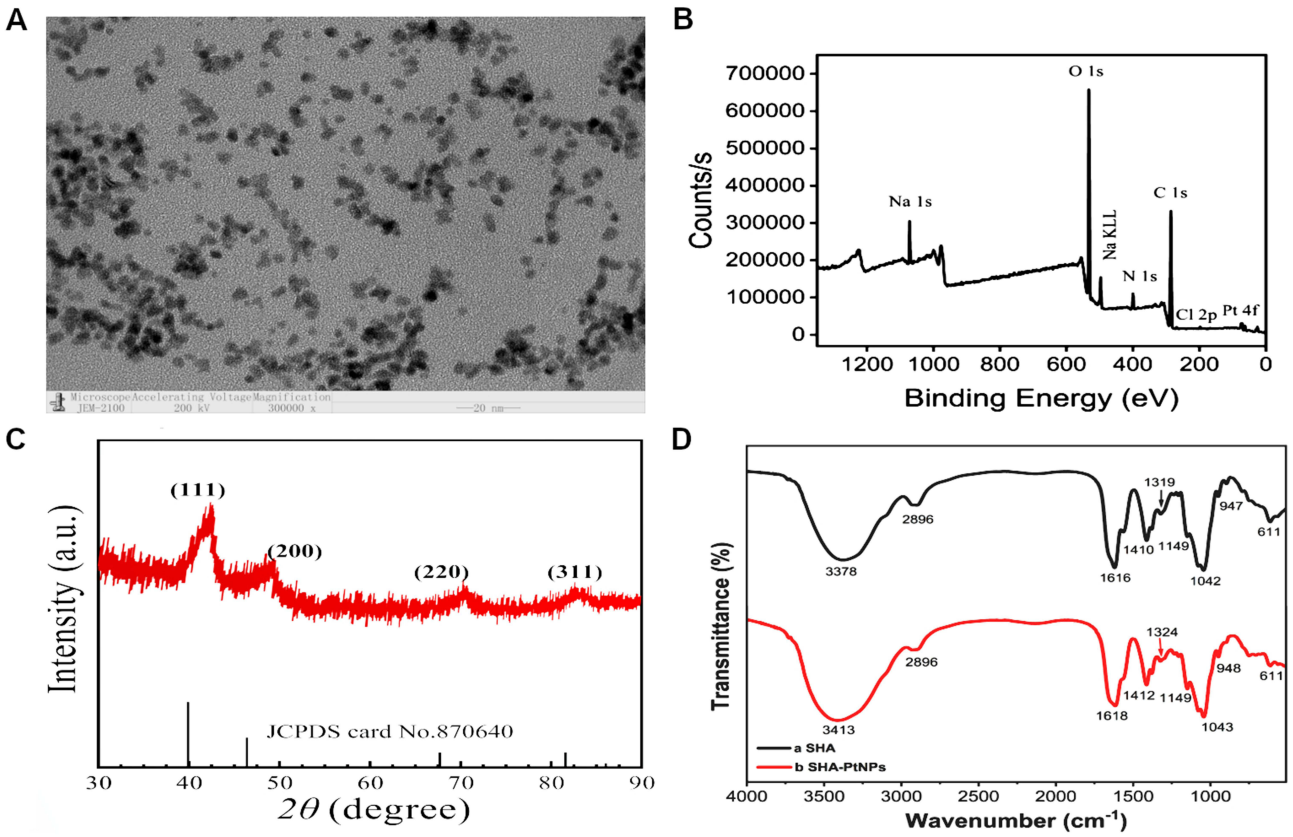

Figure 1 (**A**) The TEM image of SHA-PtNPs. (**B**) The XPS spectra of SHA-PtNPs. (**C**) The XRD patterns of SHA-PtNPs. (**D**) The FTIR spectra of SHA-PtNPs.

https://doi.org/10.2147/IJN.S586975

the treatment of chronic diabetic wounds. To validate this, a diabetic rat wound model was utilized to evaluate the wound-healing efficacy of SHA-PtNPs in vivo. The experimental flow chart is illustrated in Figure 2A. All rats survived without severe complications in the study. The various treatments (NS, SHA or SHA-PtNPs) were performed and macroscopic images and healing trajectories at designated time points provided a visual representation of the therapeutic effects (Figure 2B and C). By day 12 post-treatment, wounds treated with SHA-PtNPs exhibited markedly smaller residual areas compared with those treated with NS or SHA, indicating a faster healing rate in the SHA-PtNPs group. Quantitatively, the residual wound areas on day 12 were (0.98 ± 0.16) cm^2 for the control group, (0.41 ± 0.19) cm^2 for the SHA group, and only (0.32 ± 0.28) cm^2 for the SHA-PtNPs group. By day 15, the SHA-PtNPs group achieved nearly complete wound closure, exhibiting the highest healing rate (97.06 ± 1.76%), and clearly outperforming the other two groups (Figure S2 and Table S1). These results indicate that both SHA and SHA-PtNPs can accelerate wound healing compared to the saline control, however, the SHA-PtNPs group achieved superior healing efficiency. Significant hypertrophic granulation, scarring, and scab formation were observed in the repaired fistulas of the CON and SHA groups. In contrast, the SHA-PtNPs group exhibited well-healed skin characterized by smooth tissue and minimal granulation hyperplasia. This enhancement can be attributed to the synergistic effect of the Pt-based nanozyme activity, which confers stronger antioxidant and pro-regenerative functions, ultimately promoting more efficient wound repair. Structural stability and biocompatibility are essential indicators for assessing the potential of the material in real-world wound-healing applications. Hence, in order to systematically evaluate the structural stability and biocompatibility of the SHA-PtNPs after exerting its wound-healing effects, in-depth structural and toxicological analyses were conducted. From the TEM images, it can be seen that the SHA-PtNPs still maintains an intact spherical morphology after interacting with the wound, demonstrating its high stability in the actual wound environment (Figure S3). Moreover, no obvious

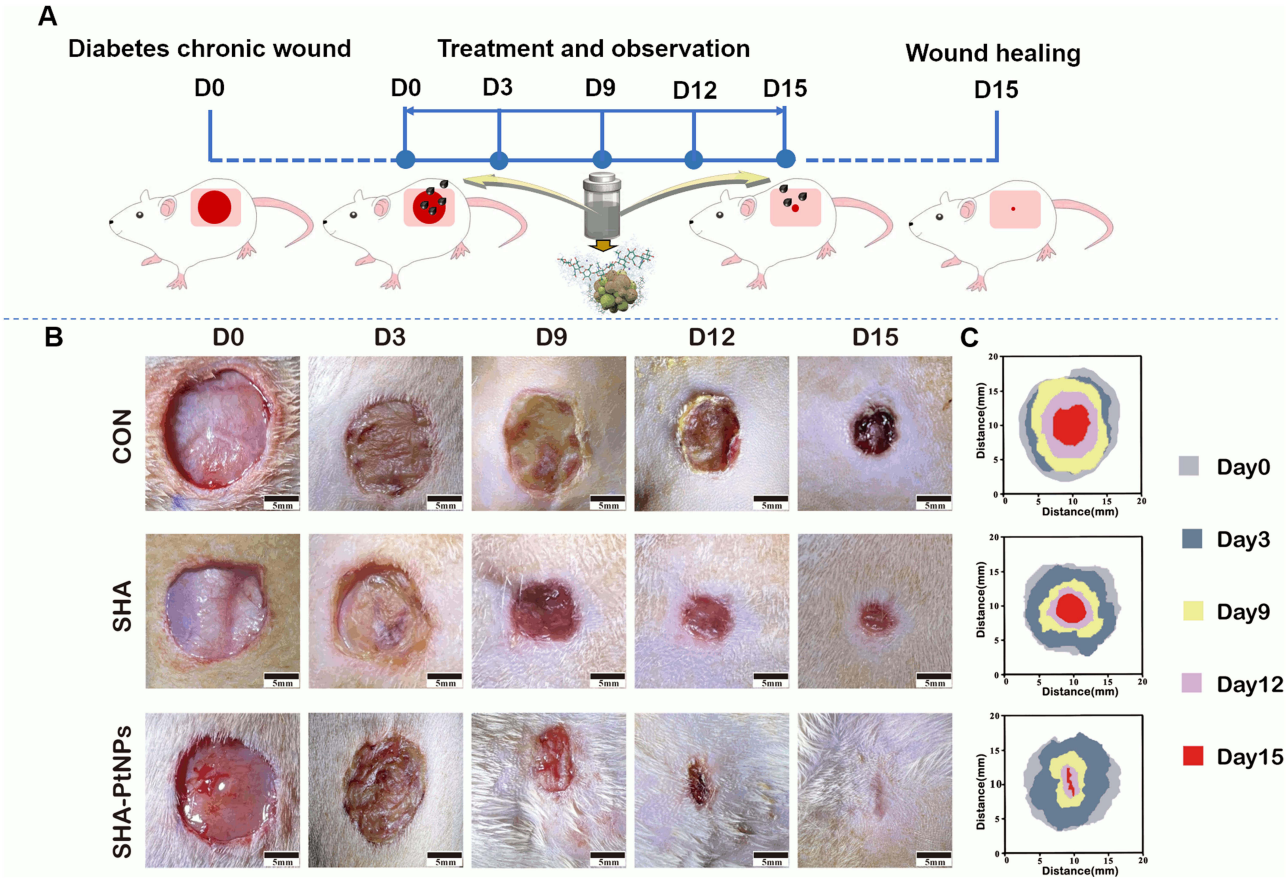

Figure 2 (**A**) Schematic illustration of the timeline of animal experiments to test the therapeutic effects of NS (CON), SHA and SHA-PtNPs. (**B**) Representative photographs of the wounds in different treatment groups (Scale bar = 5 mm). (**C**) Wound closure trace of in each group.

https://doi.org/10.2147/IJN.S586975

pathological damages were observed in the H&E staining of major organs, including the heart, lung, liver, spleen, and kidney (Figure S4). Serum biochemical markers at day 28 revealed no marked alterations in key serum biochemical parameters, Alanine Aminotransferase (ALT) and Aminotransferase (AST) for liver function, serum creatinine (SCr) and Blood urea nitrogen (BUN) for renal function, suggesting an absence of significant hepatorenal toxicity following SHA-PtNPs treatment (Figure S5 and Table S2). These findings demonstrate that SHA-PtNPs effectively promote wound healing without causing appreciable cellular or organ toxicity.

Histological Evaluation of Wound Healing

Wound healing is a complex biological process through which damaged tissues are repaired, typically proceeding through three overlapping stages: inflammation, proliferation, and remodeling.[40] During the inflammatory phase, necrotic tissues are removed and growth factors are released. The proliferative phase involves angiogenesis, granulation tissue formation, and epithelial cell migration, all of which contribute to wound closure. In the remodeling phase, collagen fibers are deposited and reorganized, leading to denser and stronger tissue architecture. The coordination among these phases ultimately restores the structural and functional integrity of the skin.[41–43] To evaluate the histological changes during the healing process, H&E staining was performed to assess inflammation, angiogenesis, granulation tissue formation, and epithelial repair. As shown in Figure 3A and Figure S6, on day 15, the CON group exhibited visible ulceration and thick scab formation (indicated by black arrows), accompanied by massive neutrophil infiltration (green circles), a few lymphocytes, granuloma formation, and no evidence of epithelial regeneration, corresponding to a high inflammation score of 3. In contrast, the SHA group showed reduced ulceration with partial necrotic scab coverage (black arrows), mild neutrophil and lymphocyte infiltration, granuloma formation, and moderate fibroblast proliferation and vessel alignment, along with limited epithelial regeneration, which was consistent with a mild inflammation score of 1.60 ± 0.55. The SHA-PtNPs group, with an inflammation score of 0, showed significantly fewer inflammatory cells and more matured fibroblasts (blue arrows) than the other groups.

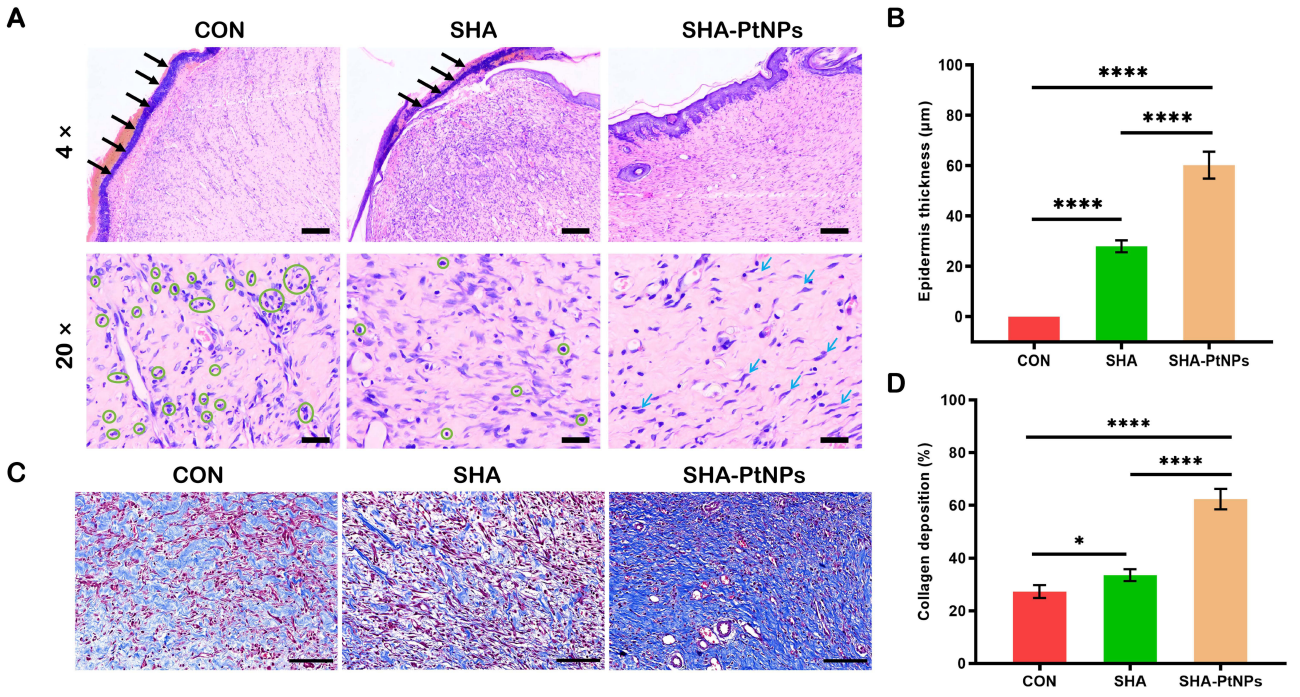

Figure 3 Histological analysis of healed wound tissue. (**A**) Representative images of H&E staining of tissues treated with NS, SHA, and SHA-PtNPs on day 15 (4×, Scale bar = 100 μm, 20×, Scale bar = 20 μm. Ulceration and thick scab formation indicated by black arrows, neutrophil infiltration marked by green circles, matured fibroblasts indicated by blue arrows.). (**B**) Quantitative analysis of regenerated epithelium thickness on the 15th day. Data are presented as mean ± SD (****P < 0.0001 compared with one-way ANOVA with Tukey's post hoc tests, n=3). (**C**) Representative images of MT staining of wound tissues treated with NS, SHA, and SHA-PtNPs on day 15 (Scale bar = 50 μm). (**D**) Quantitative analysis of collagen deposition on the 15th day. Data are presented as mean ± SD (*P < 0.05, ****P < 0.0001 compared with one-way ANOVA with Tukey's post hoc tests, n=3).

https://doi.org/10.2147/IJN.S586975

Further histological comparison among the three groups on days 9, 15 and 28 provided additional evidence of accelerated healing in the SHA-PtNPs group. On day 9, the CON group displayed massive neutrophil infiltration, while the SHA group showed lymphocyte infiltration, granuloma formation, and fibroblast proliferation. The SHA-PtNPs group exhibited fewer neutrophils, noticeable fibroblast proliferation, aligned neovascular structures, and mild epithelial regeneration (Figure S7). At day 15, no discernible epidermal layer was observed in the CON group, suggesting that re-epithelialization had not yet been effectively established. The SHA group developed a thin and immature neo-epidermis, with a measured thickness of approximately 27.95 ± 2.11 μm, reflecting limited regenerative progression. The SHA-PtNPs group exhibited a markedly thicker epidermal layer, reaching approximately 60.22 ± 4.77 μm, indicative of more robust epidermal reconstruction and a faster healing trajectory relative to the other groups (Figure 3B). By day 28, the CON group displayed complete but disorganized epithelium with irregular fibroblast alignment, poor healing quality by attenuated epidermis thickness (29.55 ± 12.08 μm), and absence of skin appendages compared with normal skin. The SHA group exhibited re-epithelialization, with newly formed epidermis of similar thickness (37.51±9.74 μm) to normal tissue, aligned fibroblasts, and several visible hair follicles. Notably, the SHA-PtNPs group showed complete re-epithelialization with epidermal thickness (78.77 ± 18.23 μm) comparable to normal skin, well-aligned fibroblasts, and the presence of sebaceous glands and hair follicles, indicating almost complete tissue restoration (Figure S8 and Figure S9). Remarkably, the SHA-PtNPs group showed complete epithelial coverage (re-epithelialization) without ulcer or scab formation, moderate lymphocyte infiltration, extensive collagen deposition, and partial scar formation within the granulation tissue. These results confirm that SHA-PtNPs significantly enhanced wound healing compared to SHA and CON groups.

In addition, collagen deposition and tissue remodeling were assessed using MT staining. On day 15, the CON group showed necrosis with limited collagen deposition and sparse collagen fibers, indicating poor healing and minimal tissue regeneration. By contrast, the SHA group exhibited a slight increase in collagen deposition, particularly around the wound edges, although the collagen fibers remained disorganized. Notably, the SHA-PtNPs group displayed significantly higher collagen deposition compared with both the SHA and CON groups ($P < 0.05$), with a well-organized and denser collagen network, suggesting substantial tissue remodeling. As shown in Figure 3C and D, collagen fibers in the SHA-PtNPs group were dense and mature. Quantitative analysis further confirmed these observations: compared with the CON (27.28 ± 2.44%) and SHA groups (33.51 ± 2.24%), the SHA-PtNPs group exhibited markedly increased collagen deposition (62.37 ± 3.85%). Since collagen proliferation plays a critical role in tissue repair quality and scar formation, these findings further confirm that SHA-PtNPs effectively promote wound healing.

Overall, wounds treated with SHA-PtNPs demonstrated markedly improved healing efficiency by reducing inflammation, stimulating re-epithelialization and collagen deposition during the process compared with those treated with SHA or saline, highlighting the strong potential of SHA-PtNPs in promoting the repair of chronic, non-healing diabetic wounds.

Mechanistic Insights into SHA-PtNPs-Promoted Wound Healing

To investigate the mechanisms by which SHA-PtNPs accelerate wound healing, several key regulatory markers involved in inflammation, angiogenesis, and tissue remodeling were analyzed, including IL-1β, IL-4, TGF-β1, CD31 and α-SMA.[44–46] IL-1β is a typical pro-inflammatory cytokine that induces fever and promotes infiltration of inflammatory cells, such as neutrophils and monocytes, with elevated levels indicating acute or chronic inflammation. As shown in Figure 4A, on day 3 during the inflammatory phase, IL-1β expression was positive in the CON group, weakly positive in the SHA group, and negative in the SHA-PtNPs group. By day 9, IL-1β remained positive in the CON and SHA groups, while it remained negative in the SHA-PtNPs group, suggesting that SHA-PtNPs effectively suppress inflammatory responses during early wound repair. Similarly, immunohistochemical (IHC) analysis of the anti-inflammatory cytokine IL-4 revealed that on day 3, IL-4 expression was nearly negative in the CON group, weak in the SHA group, and relatively high in the SHA-PtNPs group (Figure 4B). By day 9, IL-4 expression was observed in all three groups, with the highest level in the SHA-PtNPs group. These findings indicate that SHA-PtNPs exerts a significant anti-inflammatory effect during the early stage of wound healing.

Re-epithelialization and granulation tissue formation are critical for wound closure. TGF-β1 is a key regulator throughout epithelialization, tissue proliferation, and remodeling, exerting anti-inflammatory effects, promoting cell proliferation and migration, and regulating collagen synthesis and deposition to maintain balanced tissue repair. In our

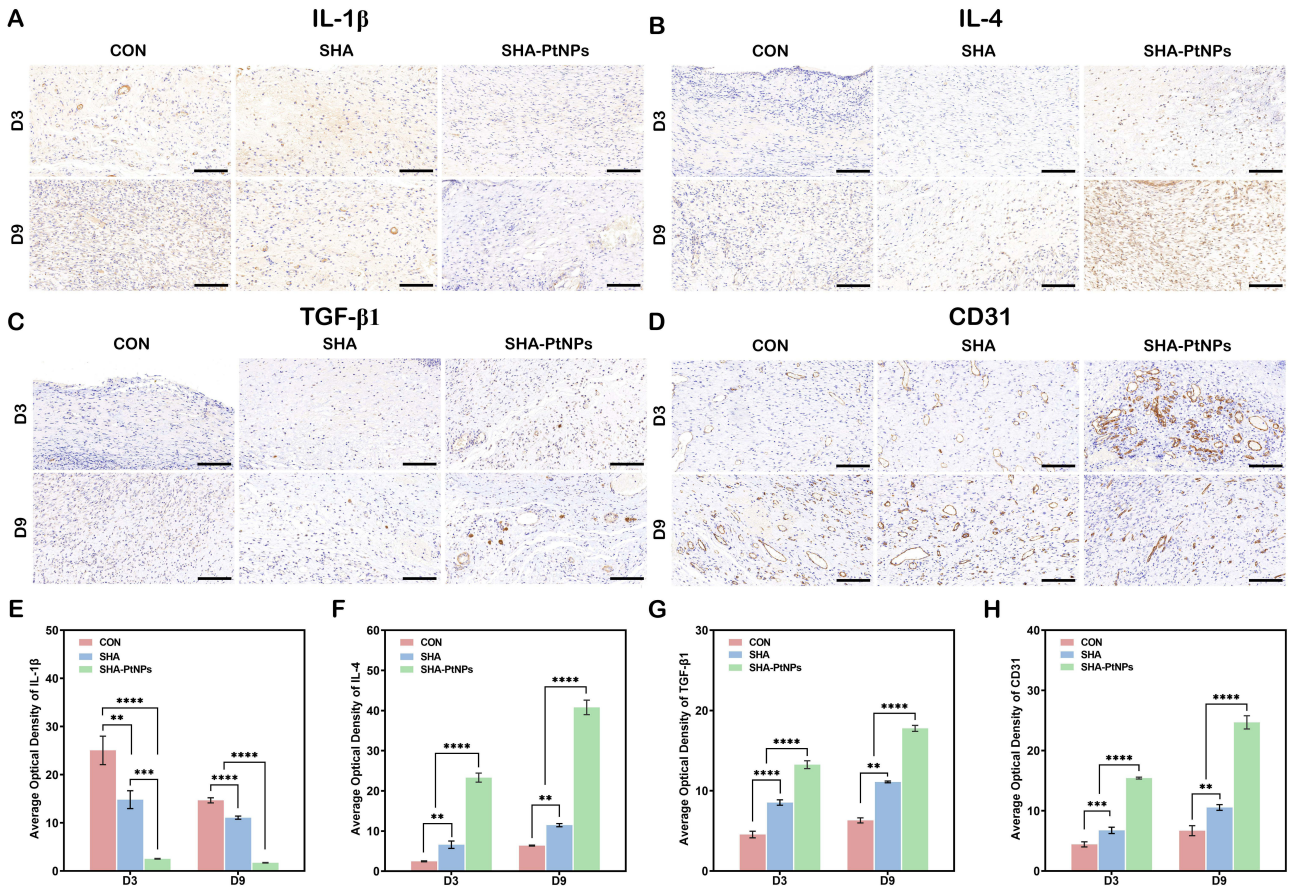

Figure 4 Anti-inflammatory activity of SHA-PtNPs for wound healing therapy. Representative images of immunohistochemistry staining of (**A**) IL-1β, (**B**) IL- 4, (**C**) TGF-β1 and (**D**) CD31 on day 3 and day 9 (Scale bars = 100 μm, n=3). Quantitative analysis of IHC for IL-1β (**E**), IL- 4 (**F**), TGF-β1 (**G**) and CD31 (**H**) on the day 3 and day 9 post-treatment. All data are presented as the mean ± SD. (**P < 0.01, ***P < 0.001, ****P < 0.0001 compared with one-way ANOVA with Tukey's post hoc tests, n=3).

study, TGF-β1 expression was detectable in the SHA-PtNPs group as early as day 3 and persisted throughout the healing process (Figure 4C). In contrast, the CON group exhibited no detectable TGF-β1 expression even on day 9, and the SHA group showed delayed TGF-β1 expression compared with SHA-PtNPs, suggesting that SHA-PtNPs may promote wound healing by modulating TGF-β1 secretion and activity. Angiogenesis was evaluated by CD31, a key endothelial marker. Elevated CD31 expression in the early stages indicates endothelial activation and neovascular formation, while gradual decline reflects vascular maturation and stabilization. On day 3, modest angiogenesis was observed in the CON group, whereas extensive neovascular formation was evident in both SHA and SHA-PtNPs groups (Figure 4D). IHC results revealed a marked downregulation of IL-1β and an upregulation of IL-4, TGF-β1, and CD31 expression in the SHA-PtNPs group compared with the other two groups (Figure 4E–H). By day 9, newly formed vessels began regressing, with the SHA-PtNPs group showing the most pronounced reduction, indicating the fastest healing progression. Myofibroblast activation was assessed via α-SMA, a marker critical for wound contraction and tissue remodeling. On day 3, α-SMA-positive cells were detected around new capillaries in all groups, with the strongest expression in the SHA-PtNPs group. By day 9, the number of α-SMA-positive cells increased and became disorganized, with the SHA-PtNPs group showing the greatest increase (Figure S10 and Figure S11), reflecting accelerated tissue remodeling and granulation maturation.

The healing of diabetic wounds poses a critical clinical challenge, as excessive and persistent inflammation induce tissue damage and delayed healing, highlighting the importance of exploring the mechanism of inflammation. Macrophages play a pivotal role in regulating the immune microenvironment and are indispensable immune cells during wound healing.[47–50] CD68 serves as a pan-macrophage surface marker, CD86 marks classically activated M1 macrophages, and CD206 marks alternatively activated M2 macrophages. Different macrophage subtypes perform distinct biological functions at different stages of healing. M1 macrophages (classically activated) identified by CD86 are primarily responsible for pathogen

https://doi.org/10.2147/IJN.S586975

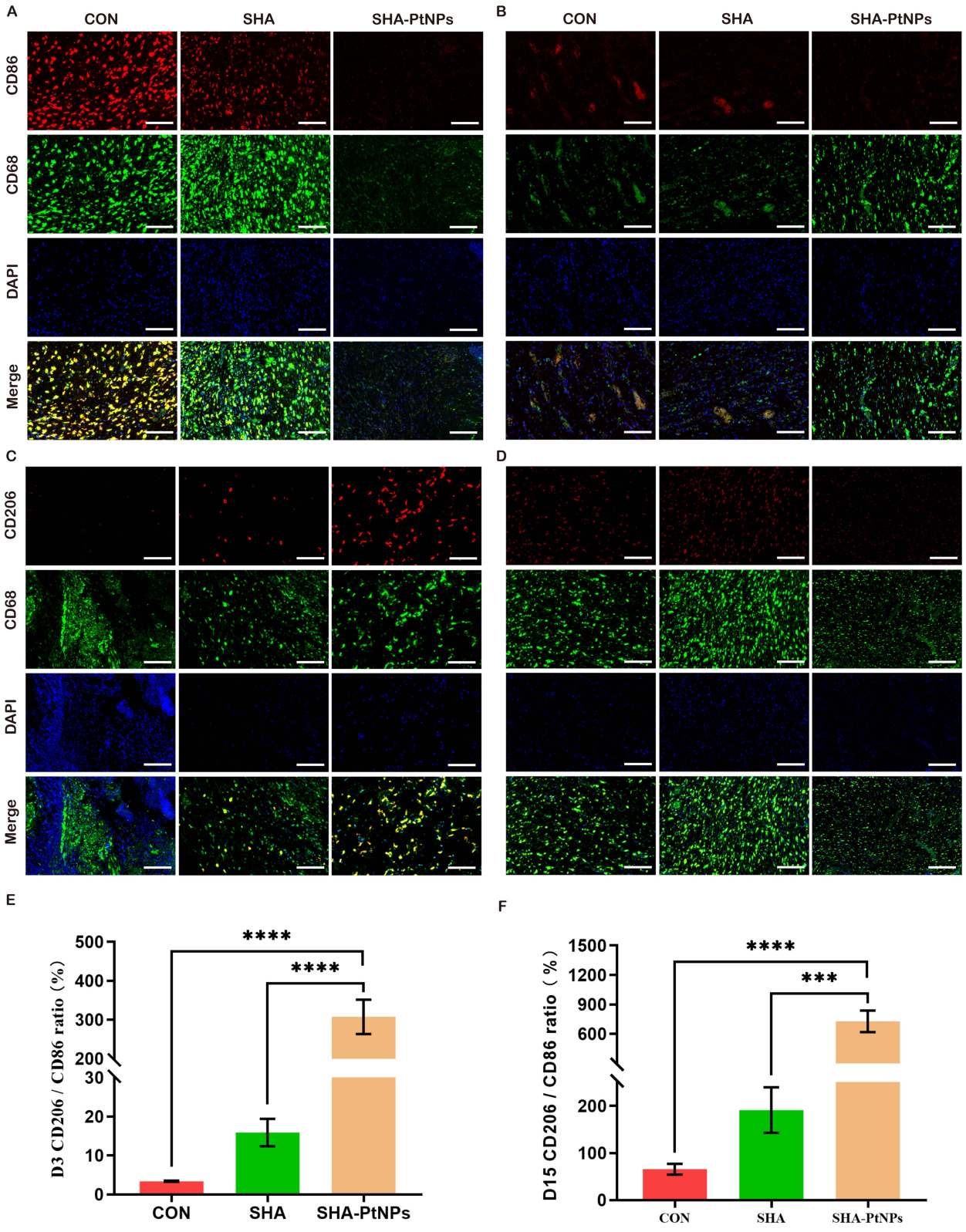

Figure 5 Regulation of macrophage polarization via SHA-PtNPs for wound healing. Representative images of immunofluorescence (IF) staining of CD86 and CD68 on day 3 (**A**) and day 15 (**B**). Representative images of immunofluorescence staining of CD206 and CD68 on day 3 (**C**) and day 15 (**D**) (Scale bars = 100 μm, n=3). Quantitative analysis of IF for the ratio of CD206/CD86 on the day 3 (**E**) and day 15 (**F**) post-treatment. All data are presented as the mean ± SD. (***P < 0.001, ****P < 0.0001 compared with one-way ANOVA with Tukey's post hoc tests, n=3).

https://doi.org/10.2147/IJN.S586975

clearance, secretion of pro-inflammatory cytokines, and promotion of Th1 immune responses, playing critical roles in early-stage anti-infection and debridement. In contrast, M2 macrophages (alternatively activated), marked by CD206, contribute to wound repair through angiogenesis, extracellular matrix remodeling, anti-inflammatory cytokine secretion, and resolution of inflammation. During wound healing, macrophages not only initiate local immune responses but also transition from the M1 to M2 phenotype, facilitating the switch from inflammation to tissue repair, a dynamic essential for inflammation control, tissue regeneration, and healing quality. As shown in Figure 5A–D, on day 3, the CON group exhibited a high number of M1 macrophages and almost no M2 macrophages. Compared with the CON and SHA groups, the SHA-PtNPs group had the fewest M1 macrophages and the most M2 macrophages, indicating that while the CON and SHA groups remained in the inflammatory phase, the SHA-PtNPs group was transitioning from inflammation to the proliferative phase. By day 15, M1 macrophages in the CON and SHA groups were significantly reduced, with a notable increase in M2 macrophages, suggesting the wounds were still in the proliferative phase. Conversely, M1 and M2 macrophages in the SHA-PtNPs group were nearly absent, indicating that the wounds were almost fully healed. The ratio of CD206/CD86 corroborated these observations from immunofluorescence staining. At both day 3 and day 15, the SHA-PtNPs group exhibited the highest CD206/CD86 ratio, reflecting an active tissue repair state and confirming the superior wound-healing efficacy of SHA-PtNPs compared to the CON and SHA groups (Figure 5E and F). In this study, we demonstrated that SHA-PtNPs effectively orchestrated macrophage polarization from a pro-inflammatory M1 phenotype toward a pro-healing M2 phenotype, thereby accelerating diabetic wound closure. Transitioning macrophages from the pro-inflammatory M1 phenotype to the anti-inflammatory M2 phenotype is key to reducing inflammation and enhancing tissue repair. The repolarization of macrophages might hold promise as a therapeutic strategy to mitigate persistent inflammation and promote tissue regeneration.

Taken together, these results demonstrate that SHA-PtNPs exhibit stronger anti-inflammatory activity than the CON and SHA groups, effectively suppressing inflammatory responses and cytokine production. Mechanistically, SHA-PtNPs act through a coordinated multi-pathway regulation: they promote TGF-β1 secretion, which contributes to tissue repair and extracellular matrix remodeling; simultaneously, they upregulate CD31 and α-SMA expression, enhancing angiogenesis and tissue contraction. In parallel, SHA-PtNPs facilitate the phenotypic transition of macrophages from the pro-inflammatory M1 state to the reparative M2 state, further mitigating inflammation and promoting tissue regeneration. This integrative regulation of inflammatory response, angiogenesis, and macrophage polarization highlights the synergistic nature of SHA-PtNPs in accelerating wound healing (Table S3). Overall, the material accelerates diabetic wound repair through the combined effects of ROS scavenging, immune modulation, and promotion of vascularization and tissue remodeling, demonstrating its high therapeutic potential and distinctive advantages over conventional nanozyme-based wound therapies.

Conclusion

In this study, we developed a nanozyme-based material, SHA-PtNPs, for promoting the healing of chronic diabetic wounds. The material exhibits excellent dispersibility and efficient enzyme-mimicking activities, including CAT-like activity (3320 U/g) and SOD-like activity (129,000 U/g), enabling the effective scavenging of various ROS, such as H_2O_2, $O_2\bullet^-$, and •OH, demonstrating superior antioxidant properties. In vivo experiments showed that the residual wound area on day 12 was 0.78 ± 0.16 cm^2 for the CON group, 0.40 ± 0.19 cm^2 for the SHA group, and only 0.32 ± 0.28 cm^2 for the SHA-PtNPs group. Importantly, the healing rate is nearly 97.06 ± 1.76% by day 15 and almost fully restored to normal skin by day 28, indicating its remarkable efficacy in accelerating chronic wound healing. Mechanistic studies further revealed that SHA-PtNPs markedly inhibit inflammatory responses and pro-inflammatory cytokine production, while promoting TGF-β1 secretion and elevating CD31 and α-SMA expression, thereby facilitating angiogenesis and tissue contraction. Furthermore, by inducing macrophage polarization from the M1 to M2 phenotype, SHA-PtNPs further reduce inflammation and enhance tissue regeneration. Based on these findings, SHA-PtNPs promote wound healing through a synergistic, multi-mechanism process, providing a promising strategy and theoretical basis for the biomedical application of nanozyme-based materials.

Funding

The authors gratefully acknowledge financial support from the Natural Science Foundation of Fujian Province (2023J01102, 2023J01741), the Joint funds for the innovation of science and technology, Fujian province (2023Y9262, 2023Y9260),

Quanzhou City Science & Technology Program of China (2025QZNY080) and the Doctoral Research Foundation Project of the Second Affiliated Hospital of Fujian Medical University (2022BD0104, 2022BD1004).

Disclosure

The authors report no conflicts of interest in this work.

References

1. Xu G, Xu P, Gao B, et al. Stimulus-responsive bioactive hydrogels in diabetic wound healing. *ACS Appl Nano Mat*. 2024;7(10):11037–11052. doi:10.1021/acsanm.4c01917
2. Marian Sue K, Hussain M, Mary TK. Intensive blood glucose control and vascular outcomes in patients with type 2 diabetes mellitus. *Endocrin Metab Clin*. 2018;47:81–96. doi:10.1016/j.ecl.2017.10.002
3. Mohamed L, Jennifer A, Huba K, et al. Chronic complications of diabetes mellitus: a mini review. *Curr Diab Rev*. 2017;13:3–10. doi:10.2174/1573399812666151016101622
4. Daiyong C, Qing D, Zhixuan Y. Specific nanodrug for diabetic chronic wounds based on antioxidase-mimicking MOF-818 nanozymes. *J Am Chem Soc*. 2022;144:23438–23447. doi:10.1021/jacs.2c09663
5. Ezhilarasu H, Vishalli D, Dheen T, et al. Nanoparticle-based therapeutic approach for diabetic wound healing. *Nanomaterials*. 2020;10:1234. doi:10.3390/nano10061234
6. Cole B, Florez C. Genetics of diabetes mellitus and diabetes complications. *Nat Rev Nephrol*. 2020;16:377–390. doi:10.1038/s41581-020-0278-5
7. Heni W, Zejun X, Meng Z, et al. Advances of hydrogel dressings in diabetic wounds. *Biomater Sci*. 2021;9:1530–1546. doi:10.1039/D0BM01747G
8. Sha L, Qingfei Z, Jie Y, et al. Absorbable thioether grafted hyaluronic acid nanofibrous hydrogel for synergistic modulation of inflammation microenvironment to accelerate chronic diabetic wound healing. *Adv Healthcare Mater*. 2020;9:2000198. doi:10.1002/adhm.202000198
9. Li-ling D, Chenzhen D, Pei-yang S, et al. The role of oxidative stress and antioxidants in diabetic wound healing. *Oxid Med Cell Longev*. 2021;11:8852759. doi:10.1155/2021/8852759
10. Chafer M, Werner S. Oxidative stress in normal and impaired wound repair. *Pharmacolog Res*. 2008;58(2):165–171. doi:10.1016/j.phrs.2008.06.004
11. Yu M, Tang P, Tang Y, et al. Breathable, moisturizing, anti-oxidation SSD-PG-PVA/KGM fibrous membranes for accelerating diabetic wound tissue regeneration. *ACS Appl Bio Mat*. 2022;5(6):2894–2901. doi:10.1021/acsabm.2c00255
12. Wenqian Z, Lang C, Yuan X, et al. Antioxidant therapy and antioxidant-related bionanomaterials in diabetic wound healing. *Front Bioeng Biotechnol*. 2021;9. doi:10.3389/fbioe.2021.707479
13. Nasr AE, Iqra Z, Saeem A, et al. Role of polyphenols, their nano-formulations, and biomaterials in diabetic wound healing. *Endocr Metab Immune*. 2024;24:626–641. doi:10.2174/0118715303242310230927104709
14. Fadilah NI, Phang SJ, Kamaruzaman N, et al. Antioxidant biomaterials in cutaneous wound healing and tissue regeneration: a critical review. *Antioxidants*. 2023;12(4):787. doi:10.3390/antiox12040787
15. Comino-Sanz IM, López-Franco MD, Castro B, et al. The role of antioxidants on wound healing: a review of the current evidence. *J Clin Med*. 2021;10(16):3558. doi:10.3390/jcm10163558
16. Qinzhou Z, Cuimin C, Yong L, et al. Metal nanoparticles: advanced and promising technology in diabetic wound therapy. *Int J Nanomed*. 2024;19:965–992. doi:10.2147/IJN.S434693
17. Mai AE, Manal AA, Promy V, et al. Synthesis and characterization of noble metal/metal oxide nanoparticles and their potential antidiabetic effect on biochemical parameters and wound healing. *Green Process Synth*. 2022;11:106–115. doi:10.1515/gps-2022-0010
18. Arfaa S, Muniba A, Qaisar M, et al. Synthesis of bimetallic oxides (SrO-CoO) nanoparticles decorated polyacrylamide hydrogels for controlled drug release and wound healing applications. *Int J Biol Macromol*. 2024;274:133194. doi:10.1016/j.ijbiomac.2024.133194
19. Sonia T, Roberta S, Federica C, et al. Polymeric based hydrogel membranes for biomedical applications. *Membranes*. 2023;13:576. doi:10.3390/membranes13060576
20. Yamei X, Qiyuan H, Zongyun W, et al. Advanced polymer hydrogels that promote diabetic ulcer healing: mechanisms, classifications, and medical applications. *Biomater Res*. 2023; 27: 36. doi:10.1186/s40824-023-00379
21. Siyao C, Hao W, Xihao P, et al. Dendritic hydrogels with robust inherent antibacterial properties for promoting bacteria-infected wound healing. *ACS Appl Mater Interfaces*. 2022;14:11144–11155. doi:10.1021/acsami.1c25014
22. Xiaoliang Q, Ying L, Yajing X, et al. Hyperthermia-enhanced immunoregulation hydrogel for oxygenation and ROS neutralization in diabetic foot ulcers. *Cell Biomater*. 2025;1:100020. doi:10.1016/j.celbio.2025.100020
23. Li-ping Z, Tian-tian M, Xiao-chun B, et al. Rational design of intelligent and multifunctional dressing to promote acute/chronic wound healing. *ACS Appl Bio Mater*. 2022;5:4055–4085. doi:10.1021/acsabm.2c00500
24. Salim U, Zahid H, Shah M, et al. Metal-Phenolic Network (MPN) modified Janus fibrous hydrogel scaffold for infected diabetic wound healing. *ACS Appl Mater Interfaces*. 2025;17:10470–10484. doi:10.1021/acsami.4c20592
25. Shaobin H, Liyong S, Zhiqiang Y, et al. Platinum nanozyme embedded in hyaluronate with multifunctional attributes synergistically promoting tracheal fistula healing. *Int J Biol Macromol*. 2025:287. 10.1016/j.ijbiomac.2024.138337.
26. Lizeng G, Jie Z, Leng N, et al. Intrinsic peroxidase-like activity of ferromagnetic nanoparticles. *Nat Nanotechnol*. 2007;2:577–583. doi:10.1038/nnano.2007.260
27. Hui W, Erkang W. Nanomaterials with enzyme-like characteristics (nanozymes): next-generation artificial enzymes. *Chem Soc Rev*. 2013;42:6060–6093. doi:10.1039/c3cs35486e
28. Shaobin H, Long M, Qionghua Z, et al. Peptide nanozymes: An emerging direction for functional enzyme mimics. *Bioact Mater*. 2024;42:284–298. doi:10.1016/j.bioactmat.2024.08.033
29. Rui L, Weiheng Z, Zhuo H, et al. Self-cascade nanozyme reactor as a cuproptosis inducer synergistic inhibition of cellular respiration boosting radioimmunotherapy. *Small*. 2024;20:2306263. doi:10.1002/smll.202306263

30. Cui L, Wenbin F, Wenxiang C, et al. Red emissive carbon dot superoxide dismutase nanozyme for bioimaging and ameliorating acute lung injury. *Adv Funct Mater*. 2023;33:2213856. doi:10.1002/adfm.202213856
31. Guoheng T, Jiuyang H, Juewen L, et al. Nanozyme for tumor therapy: surface modification matters. *Exploration*. 2021;1:75–89. doi:10.1002/EXP.20210005
32. Yujie Z, Jingjie Z, Lingmin Z, et al. A cascade nanoreactor for enhancing sonodynamic therapy on colorectal cancer via synergistic ROS augment and autophagy blockage. *Nano Today*. 2023;49:101798. doi:10.1016/j.nantod.2023.101798
33. Wei J, Qing L, Ruofei Z, et al. Chiral metal-organic frameworks incorporating nanozymes as neuroinflammation inhibitors for managing Parkinson's disease. *NatCommun*. 2023;14:8137. doi:10.1038/s41467-023-43870-3
34. Ji Y, Ruofei Z, Hanqing Z, et al. Bioinspired copper single-atom nanozyme as a superoxide dismutase-like antioxidant for sepsis treatment. *Exploration*. 2022;2:20210267. doi:10.1002/EXP.20210267
35. Wei J, Xinyue H, Yuanbo Q, et al. pH-activatable pre-nanozyme mediated H2S delivery for endo-exogenous regulation of oxidative stress in acute kidney injury. *Adv Sci*. 2024;11:2303901. doi:10.1002/advs.202303901
36. Jinze W, Haiqi Z, Sentao H, et al. A MMP9-responsive nanozyme hydrogel to promote diabetic wound healing by reconstructing the balance of pro-inflammation and anti-inflammation. *J Mater Chem B*. 2025;13:8083–8093. doi:10.1039/D4TB02857K
37. Pu C, Wang Y, Xiang H, et al. Zinc-based polyoxometalate nanozyme functionalized hydrogels for optimizing the hyperglycemic-immune microenvironment to promote diabetic wound regeneration. *J Nanobiotechnol*. 2024;22:611. doi:10.1186/s12951-024-02840-7
38. Zhihao S, Lei D, Xiaowan F, et al. Nanozyme cryogel accelerates diabetic wound healing by targeting biofilms and inflammations of the wound bed. *ACS Nano*. 2025;19:35081–35101. doi:10.1021/acsnano.5c12513
39. Gupta A, Kumar P. Assessment of the histological state of the healing wound. *Plast Aesthet Res*. 2015;2:239. doi:10.4103/2347-9264.158862
40. Gurvinder K, Ganesh N, Deepa G, et al. Biomaterials-based regenerative strategies for skin tissue wound healing. *ACS Appl Bio Mater*. 2022;5:2069–2106. doi:10.1021/acsabm.2c00035
41. E SA, Paul M, Marjana T. Wound repair and regeneration: mechanisms, signaling, and translation. *Sci Transl Med*. 2014;6:265. doi:10.1126/scitranslmed.3009337
42. P OA, Paul M. Cellular and molecular mechanisms of skin wound healing. *Nat Rev Mol Cell Biol*. 2024;8:599–616. doi:10.1038/s41580-024-00715-1
43. Holly N, Matthew J. Wound healing: cellular mechanisms and pathological outcomes. *Open Biol*. 2020;10:200223. doi:10.1098/rsob.200223
44. Nidhi Y, Manju S, Deependra S, et al. Mechanistic insights of diabetic wound: Healing process, associated pathways and microRNA-based delivery systems. *Int J Pharm*. 2025. doi:10.1016/j.ijpharm.2024.125117
45. Judith E. IL-4 and IL-13: regulators and effectors of wound repair. *Annu Rev Immunol*. 2023;41:229–254. doi:10.1146/annurev-immunol-101921-041206
46. Agung P, Iffan A, Nurfitriani H, et al. MSC-released TGF-β regulate α-SMA expression of myofibroblast during wound healing. *J Stem Cells Regen Med*. 2020;16:73–79. doi:10.46582/jsrm.1602011
47. Yumi K, Yuko I, Akiko I, et al. Macrophage polarity and wound age determination. *Sci Rep*. 2022;12:20327. doi:10.1038/s41598-022-24577-9
48. Meng Z, Jinzhao O, Yuzhou C, et al. Programming of macrophage polarization in different stages for accelerating wound healing. *Chem Eng J*. 2024;491:152131. doi:10.1016/j.cej.2024.152131
49. Lan L, Yanqin Q, Zehui G, et al. Effective-components combination improves airway remodeling in COPD rats by suppressing M2 macrophage polarization via the inhibition of mTORC2 activity. *Phytomedicine*. 2021;92:153759. doi:10.1016/j.phymed.2021.153759
50. Rui C, Chengyu D, Pengwei L. Dimeric copper peptide incorporated hydrogel for promoting diabetic wound healing. *Nat. Commun*. 2025;16:5797. doi:10.1038/s41467-025-61141-1